Optical Wavelength and Dimensions Tolerance Criterion for Multimode Interference Couplers

ABDULAZIZ M. AL-HETAR[a,*], AND ZAID A. SHAMSAN[a,b]

[a]*Communications and Computer Department, Al-Saeed Faculty of Engineering and Information Technology, Taiz University, Taiz, Yemen*
[b]Deanship of Academic Research, Al-Imam Muhammad ibn Saud Islamic University, Riyadh, Saudi Arabia
alhetaraziz@gmail.com, shamsan22@gmail.com

Abstract: - The self-imaging property of a homogeneous multi-moded planar optical waveguide has been applied in the design optical couplers based on multimode Interference (MMI). Based on this design, the optical wavelength and dimensions tolerance for MMI-3dB couplers are investigated analytically. They are shown to be inversely proportional to the multimode section width. Among Symmetrical, paired, and general mechanism interference types, the symmetrical one has the highest optical wavelength and dimensions tolerance.

Key-Words: MMI coupler, Power splitter, Bandwidth, Polarization, and Self-image

1 Introduction

Optical couplers and splitters play very important roles in an optical system, especially in emerging passive optical networks for broadband access. They currently represent the largest market for photonic integrated circuit and find use in broadcast types optical networks and for optical signal routing and processing. Many kinds of planar waveguide devices can be used as power splitter, such as Star couplers [1], Y (or X) splitters [2] directional couplers [3], and multimode interference (MMI) waveguides [4-6].

Devices based on MMI are potential choices, because MMI devices have advantage of low loss, polarization independence [4], compact size, and low fabrication cost [7]. However, MMI devices are wavelength-sensitive. Variation of signal wavelength may have a significant influence on the performance of the device. To have a wide band MMI device is then of great interest for study.

The aim of this paper is to study the bandwidth capabilities of the optical power splitter based on MMI and to quantify their fabrication tolerance. In section 2, we introduce the principal operation of MMI. Fabrication tolerance and bandwidth are investigated and discussed in Sections 3. The relative phases of the MMI images are modeled and presented in Section 4.

2 Principal operation of MMI

The principal operation of MMI coupler is based on the self-imaging effect in a multimode section [8]. Fig. 1 is a top view of symmetrical, paired, and general interference of 1×2 power splitter, which is showing the positions of the input and output waveguides.

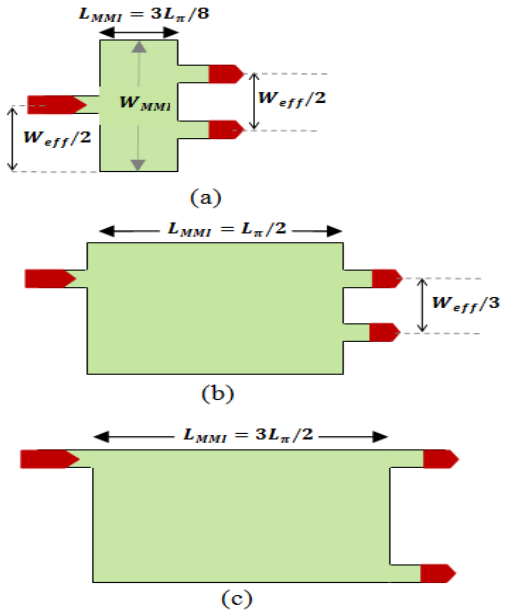

Fig.1 Schematic diagram of 1×2 power splitter in (a) Symmetrical, (b) Paired, and (c) General Interference.

The beat length and effective width of MMI section are given by [4]

$$L_\pi = \frac{\pi}{\beta_0 - \beta_1} \cong \frac{4 n_2 W_{eff}^2}{3\lambda} \quad (1)$$

$$W_{eff} = W_{MMI} + \left(\frac{\lambda}{\pi}\right)\left(\frac{n_1}{n_2}\right)^2 (n_2^2 - n_1^2)^{-0.5} \quad (2)$$

where

L_π beat (coupling) length (μm) between the two lowest order modes
W_{eff} the effective width of MMI coupler (μm)
W_{MMI} the physical width of MMI coupler (μm)
n_2 the refractive index of the guiding film
n_1 the refractive index of cladding layer
λ the operation wavelength (μm).

3 Dimensions tolerance

Relaxed tolerances are important for fabrication as well as for operating conditions. Fabrication tolerances refer to the control of the geometrical dimensions during processing and its subsequent impact on device performance. Operation tolerances relate to the device behavior for changes in the wavelength, polarization, temperature, input field distribution, and refractive index.

A tolerance analysis can be performed [9] in which each image is considered as a Gaussian beam focused at a self-image distance $z = L$. Then, the loss penalty produced by a (small) finite shift δL in the z-position of the output waveguides can be evaluated by overlapping the defocused beam with the output waveguide mode field. It is found that the length shift which produces a 0.5dB loss penalty is approximately equal to the so-called Rayleigh range [4]:

$$\delta L(\mu m) \cong \frac{\pi n_2 w_0^2}{4\lambda} \quad (3)$$

where w_0 is defined here as the Gaussian beam waist, and equals the full *l/e* amplitude width of the input field *f(x)* [9]. Eq. (3) can be interpreted as an absolute length tolerance, which does not depend on the dimensions of the multimode waveguide. An important conclusion is that, for a given wavelength and technology, all tolerances can be relaxed by using wider access waveguides. The tolerances corresponding to other fabrication or operation parameters can now be related to δL, using the definition of (1)

$$\frac{\delta L}{L} = 2\frac{\delta W_{eff}}{W_{eff}} \cong \frac{|\delta\lambda|}{\lambda} \cong \frac{\delta n_2}{n_2} \quad (4)$$

where δL, δW_{eff}, and δn_2 factors are fabrications determines. The normalized power transmission of the Gaussian beam will be calculated at a deviation distance δL from the original image distance, say α=0. It can be shown that the transmission (T) becomes as the following [10]:

$$T = \frac{1}{\sqrt{1+\alpha^2}} \quad (5)$$

$$\alpha = \frac{2\lambda\delta L}{\pi n_2 w_o^2} \quad (6)$$

$$EL = 10log_{10}(T) \quad (7)$$

An excess loss value (EL) is required to analyze the transmission loss (Loss = 0 dB at T=1) represented by a decibel value of T.

In this section, the given information are n_2=1.48, n_1=1.378, $\lambda = 1.55$ μm, h (thickness of core) = 1 μm, $W = 8$ μm . Fig. 2 shows excess loss with the fabrication tolerance of δL and its behavior is independent of the type of imaging. For a -0.5 dB loss tolerance (~90% transmission), δL can be as large as 10μm.

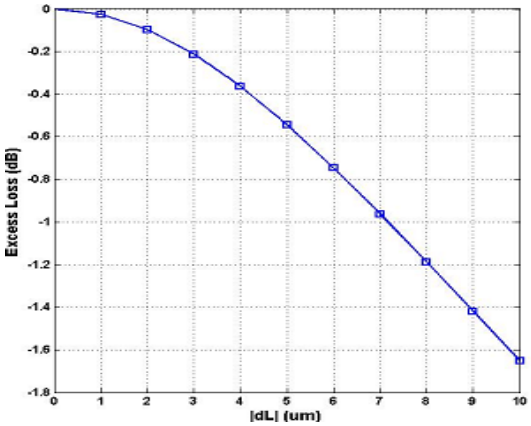

Fig.2 Dimension Tolerance δL

For deviation in width (nominal=8 μm) shown in Fig. 3, symmetrical imaging has greater width tolerance than paired or general imaging. For 1×2 images, -0.5 dB symmetrical imaging loss tolerance is nearly 1.4 μm while paired and general imaging tolerance are 0.8 μm and 0.4 μm, respectively. Symmetrical images not only offer short image distances, they also offer higher fabrication tolerances.

For the change in guide index (nominal =1.48) shown in Fig. 4 , symmetrical 1×2 imaging at -0.5 dB loss has an index tolerance of 0.42 while at the same

loss, the index tolerances are 0.3 and 0.1 for paired and general imaging, respectively. Thus, these large guide index changes in a practical system can be neglected since they should not occur under normal condition.

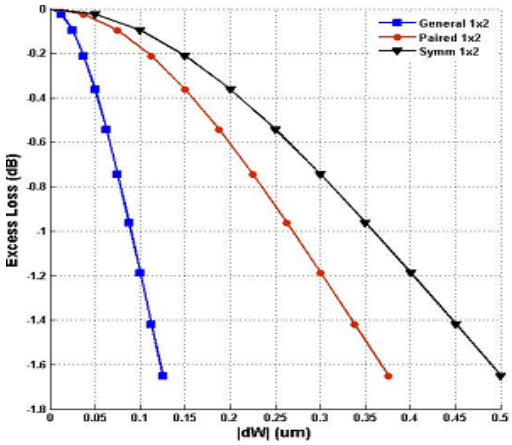

Fig.3 MMI Dimension tolerance W

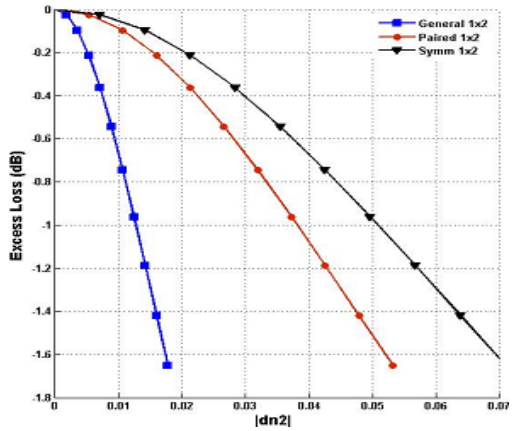

Fig. 4 Fabrication tolerance n_2

The approach adjusts the width and length of the multimode waveguide to achieve optimal device performance. It has shown that the length of the multimode waveguide can be varied in a well-defined range to find optimal device performance. In the numerical analysis, it was found that optimal performance could be achieved for various length/width combinations. Moreover, it was shown that not only the length but also the width of MMI coupler should be adjusted to achieve both low loss and good uniformity.

Optical bandwidth represents a band of transmittable wavelength under a tolerance of EL and is simply 2 times the tolerance of $|\delta\lambda|$. This value can also be obtained with relationship in Eq. (4). Thus, a similar plot can be generated with the three types of imaging shown in Fig. 5. For a transmission tolerance of 90% or -0.5dB loss, symmetrical 1×2 produces a bandwidth of *75nm* around the nominal value of 1.55μm while they are *40nm* and *18nm* for paired and general images.

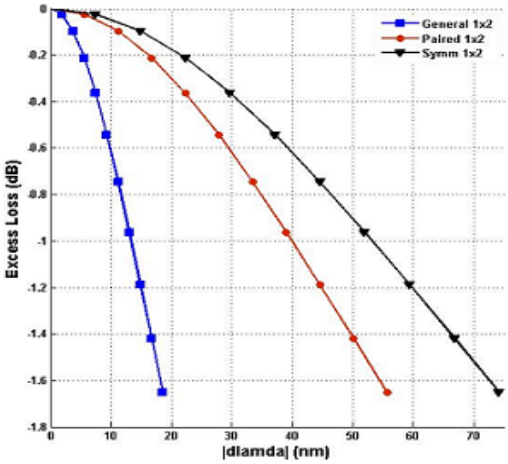

Fig.5 Optical Wavelength

4 Relative phases of the MMI images

The information of the image position in the *x* direction and phases of the output images is very important. One needs to know where multi-images appear in order to design output waveguides to capture the optical output. Furthermore, phase information of the spot images or output images is important for such devices as MMI switch or Generalized Mach-Zehnder Interferometers for optical switching. It can be shown that the field in the multimode region will be of the form [9]

$$f\left(x, L_N^b\right) = \frac{1}{C}\sum_{p=0}^{N-1} f_{in}\left(x - x_p\right).e^{j\varphi_p} \quad (8)$$

with

$$x_p = b(2p - N)\frac{W_{eff}}{N} \quad (9)$$

$$\varphi_p = b(N - p)\frac{p\pi}{N} \quad (10)$$

$$|C| = \sqrt{N} \quad (11)$$

where $f_{in}(x)$ describes the field profile at the input of the multimode region, C is a complex normalization constant, and x_p and φ_p describe the positions and phases, respectively, of N self-images at the output of the MMI coupler. The self-images are positioned with a constant spacing between them. Also p denotes the output image number. The parameter b describes a multiple of the imaging length that also results in N self-images, since the self-imaging phenomenon is periodic. Usually the shortest devices are obtained

when b=1. These positions and phases are dependent on the geometry of the MMI section, the material system, and the input waveguide placement. The MMI coupler is divided into small parts and each part has length $3L_\pi/2N$, therefore, the numbers of these parts are $2N$. A matrix equation (12) shows the relation between the magnitude and phase of self-image after one part and input field.

$$\overrightarrow{E_o} = M.\overrightarrow{E_{in}} \quad (12)$$

$$\overrightarrow{E_{in}} = \begin{vmatrix} E_{in,1} \\ : \\ E_{inN-1} \end{vmatrix} \quad , \quad \overrightarrow{E_o} = \begin{vmatrix} E_{o,1} \\ : \\ E_{o,N-1} \end{vmatrix} \quad (13)$$

$$M_{io} = 2j\frac{e^{j\frac{\pi}{4}}}{\sqrt{2N}}.sin\left(\frac{\pi io}{N}\right).\mathrm{e}^{-j\frac{\pi(i^2+o^2)}{2N}} \quad (14)$$

where $\overrightarrow{E_o}$ and $\overrightarrow{E_{in}}$ are N-1 dimensional vectors, and M is $(N-1)\times(N-1)$ matrices. $\vec{E}$ and $\overrightarrow{E_{in}}$ describe the field amplitudes at the N-1 input and output ports, respectively. The matrix M describes the mapping of the field from the input to the length of MMI equal to $3L_\pi/2N$, and $j=\sqrt{-1}$. If the actual ports are 4, for covering the theory of this approach and identifying with standard theory of MMI, $N=8$ as shown in the Fig. 6. The actual ports are 4

$$M = \begin{vmatrix} M_{1,1} & .. & M_{1,N-1} \\ : & : & : \\ M_{N-1,1} & .. & M_{N-1,N-1} \end{vmatrix} = \begin{vmatrix} M_{1,1} & .. & M_{1,7} \\ : & : & : \\ M_{7,1} & .. & M_{7,7} \end{vmatrix} \quad (15)$$

$$\overrightarrow{E_o} = M^{2N}.\overrightarrow{E_{in}} = M^{16}.\overrightarrow{E_{in}} \quad (16)$$

The port number 1, 3, 5, and 7 are used to form 4×4 MMI coupler.

An optical field entering the MMI coupler from the input ports $i=1, 2, 3$ and 4 result in four self-image fields which are equal in magnitude for each after distance $z=3L_\pi/4$, and 9Lπ/4 with relative phases as shown in Table 3.2, calculated using Eq. (16). Note that from Table. 1 each input port imparts its own characteristic relative phase distribution to the self-image, and that the distribution differs in general for different input ports.

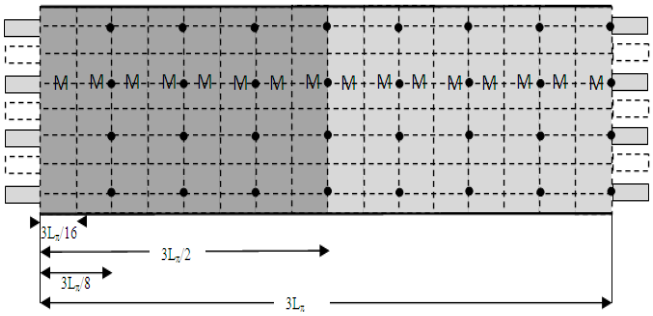

Fig. 6 Geometry of a 4×4 MMI coupler

Table 1 The magnitudes and relative phases of the self-images along of MMI's length

In	Out	$M^2(3L_\pi/8)$	$M^2(3L_\pi/8)$	$M^2(3L_\pi/8)$	$M^2(3L_\pi/8)$
Length		$3L_\pi/4$	$3L_\pi/2$	$18L_\pi/8$	$3L_\pi$
1	1	$0.5\angle45^\circ$	$0.707\angle45^\circ$	$0.5\angle135^\circ$	0
	2	$0.5\angle180^\circ$	0	$0.5\angle180^\circ$	0
	3	$0.5\angle0^\circ$	0	$0.5\angle0^\circ$	0
	4	$0.5\angle45^\circ$	$0.707\angle135$	$0.5\angle135^\circ$	1
2	1	$0.5\angle180^\circ$	0	$0.5\angle180^\circ$	0
	2	$0.5\angle45^\circ$	$0.707\angle45^\circ$	$0.5\angle135^\circ$	0
	3	$0.5\angle45^\circ$	$0.707\angle135$	$0.5\angle135^\circ$	1
	4	$0.5\angle0^\circ$	0	$0.5\angle0^\circ$	0
3	1	$0.5\angle0^\circ$	0	$0.5\angle0^\circ$	0
	2	$0.5\angle45^\circ$	$0.707\angle135$	$0.5\angle135^\circ$	1
	3	$0.5\angle45^\circ$	$0.707\angle45^\circ$	$0.5\angle135^\circ$	0
	4	$0.5\angle180^\circ$	0	$0.5\angle180^\circ$	0
4	1	$0.5\angle45^\circ$	$0.707\angle135$	$0.5\angle135^\circ$	1
	2	$0.5\angle0^\circ$	0	$0.5\angle0^\circ$	0
	3	$0.5\angle180^\circ$	0	$0.5\angle180^\circ$	0
	4	$0.5\angle45^\circ$	$0.707\angle45^\circ$	$0.5\angle135^\circ$	0

To see how the phase properties of the $N\times N$ MMI coupler can be useful, consider as an example the operation of the 4×4 MMI coupler shown in Fig. 7

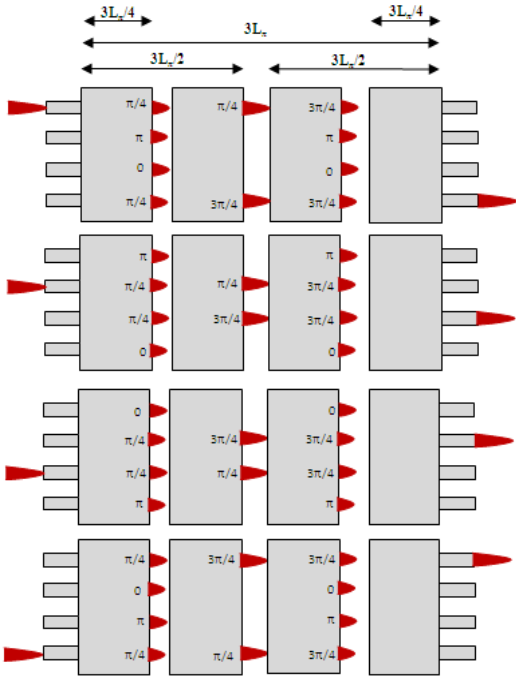

Fig. 7 Theoretical diagram of the light propagation through self-imaging multimode waveguide.

Now in order to route the input field back to the same port, instead of reversing the direction of the field, which is a difficult function to achieve in integrated optics, the MMI coupler is divided to four parts as shown in Fig.7. If an input of the first MMI coupler is to be routed to the same output port number of the fourth part in the MMI coupler, the sign of the phases of the self-images must be reversed before they enter the third part of MMI coupler. Reversing the sign results ensures the cancellation of the accumulated phase dispersion among the modes as they travel back through the multimode region, so that they reconstruct the original input field. In the other meaning, either phase of the self-images must be changed by π before it enters the third part of MMI coupler.

5 Conclusion

The self-imaging property of a homogeneous multi-moded planar optical waveguide has been applied in the design optical couplers based on multimode Interference (MMI). Based on this design, the optical wavelength and dimensions tolerance for MMI-3dB couplers were investigated analytically. They have been shown to be inversely proportional to the multimode section width. Among symmetrical, paired, and general mechanism interference types, the symmetrical one has the highest optical wavelength and dimensions tolerance. The mathematical modeling has been coded to illustrate the mechanisms of forming these images, and calculate the relative phases of the multimode images.

References

[1] C. Dragone, C. H. Henry, I. P. Kaminow, and R. C. Kistler, "Efficient multichannel integrated optics star coupler on silicon," *IEEE Photon. Technol. Lett.*, 1999, 1(8), pp. 241–243.

[2] C. Chaudhari, D. S. Patil, and D. K. Gautam, "A new technique for the reduction of the power loss in the Y-branch optical power splitter," *Opt. Commun.*, 2001, vol. 193, pp. 121–125.

[3] K. Kishioka, " A design method to achieve wide wavelength-flattened responses in the directional coupler-type optical power splitter," *J. Lightw. Technol.*, 2001, 19(11), pp. 1705-1715.

[4] L. B. Soldano and E. C. M. Pennings, "Optical multi-mode interference devices based on self-imaging: Principles and applications," *J. Lightw. Technol.*, 1995, 13(4), pp. 615–627.

[5] Y. Ma, S. Park, L. Wang, and S. T. Ho, "Ultracompact multimode interference 3-dB coupler with strong lateral confinement by deep dry etching," *IEEE Photon. Technol. Lett.*, 2000, 12(5), pp. 492–494.

[6] Abdulaziz M. Al-hetar, Abu Sahmah Bin Mohd Supa'at, N. M. Kassim and A. B. Mohammad " Design and optimization of optical power splitter based on multimode interference for 1.55-μm operation" Applied Electromagnetics, 2007. APACE 2007. Asia-Pacific Conference , Malaysia, 4-6 Dec. 2007, pp. 1 – 4.

[7] Hung-Chih Lu, and Way-Seen Wang, "Wideband Criterion for multimode interference splitters" *IEEE Photonics Technology Letters*, 2006, 18(22), pp. 2332-2334.

[8] Bryngdahl, O." Image formation using self-imaging techniques" *J. Opt. Soc. Amer. 1973*, 63(4),pp. 416-419.

[9] Besse, P. A., Bachmann, M., Melchior, H., Soldano, L. B., and Smit, M. K , "Optical bandwidth and fabrication tolerances of multimode interference couplers" *J. Lightw. Technol., 1994*, 12(6), 1004–1009.

[10] Xie Nan , "Three Dimensional Multimode Interference for optical layer routing" Master Thesis. University of Alberta. Alberta, Canada, 2006.